The VLA Expansion Project Memo Series

Number 20

Configuration Studies For the Expanded Very Large Array

Aaron Cohen
Rick Perley

4 December 2000

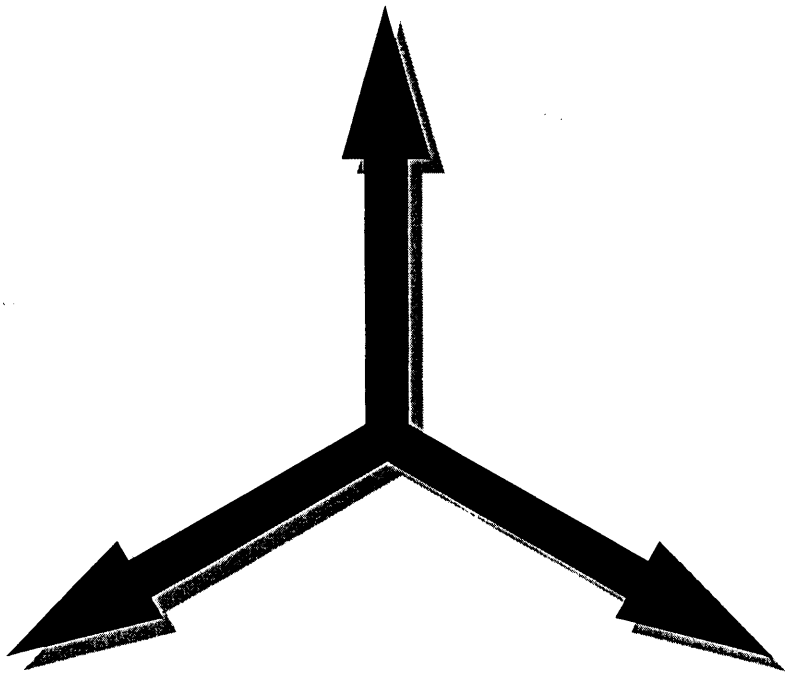

Returning the Instrument to the State of the Art

National Radio Astronomy Observatory

VLA Expansion Project Memorandum #20

Configuration Studies for the Expanded Very Large Array

Aaron Cohen and Rick Perley
December 4, 2000

1 Introduction

A key goal of the Expanded VLA Project is to increase the resolution of the Very Large Array through the addition of new antennas at distances of up to $\sim$ 250 km from the array center. These new antennas, plus two or three of the nearest VLBA antennas, would comprise a new configuration – 'The New Mexico Array', which could be used as a stand-alone array, or in combination with some or all of the present VLA's antennas, to provide a powerful and flexible array with approximately ten times the resolution of the present **A**-configuration.

A critical characteristic for any new array or configuration is its imaging performance for complex objects that the telescope may be required to observe. For the proposed 'New Mexico Array, it is important to estimate the imaging performance as a function of the number and location of the proposed new antennas.

This memo reports the results of a study to estimate the imaging performance of the proposed expanded array for one class of location geometry – a pair of rings surrounding the present VLA – as a function of the number of new antennas. The imaging characteristics of other proposed geometries have been explored by Holdaway and Perley (EVLA Memo #7) and by Keto (EVLA Memo #9). The imaging metrics used by these memos differ from those utilized here, and a later memo will undertake a comparison.

2 Choice of Array Geometry

The geometry adopted for this study consists of two rings, an inner ring of diameter 100 km which includes the VLBA's PT antenna, and an outer ring of diameter 360 km which includes the VLBA's LA antenna. This particular geometry was selected because of its simplicity and because a continuous ring distribution provides a completely uniform sampling of the *(u,v)* plane. On the inner ring, we place two new antennas (for a total of three), and on the outer, we place from 2 to 13 new antennas (for a total of 3 to 14). As the outer ring is constrained to pass through the VLBA's Los Alamos station, its center must lie on an arc of radius 180 km from the LA station. A number of trials for the best center location were conducted. The results reported here were made with the center located east of the array, approximately 20 km north of Socorro. The two new inner-ring antennas were placed so to best fill gaps in the spatial coverage on scales from 30 to 50 km. No optimization of their position was attempted in this study.

The outer-ring antennas were placed evenly around the ring without regard to actual ground location. Experience shows that position modifications which are small compared to the scale of the distribution have little effect on the imaging characteristics. Clearly, any final design will take into account such practical matters as road access, power, land usage, etc.

Experience also demonstrates that a concentration of shorter spacings is beneficial for imaging complicated, extended objects. For the EVLA, this will automatically be provided by the concentration of 27 antennas in the existing A-configuration. Such a dense concentration actually causes difficulties in image deconvolution, which can be partially alleviated by robust weighting schemes at the cost of decreased point-source sensitivity.

Two examples of the array geometry and resulting aperture plane coverage of the proposed array are shown in Figures 1 and 2.

It is anticipated that an extended, fixed configuration of new antennas will be flexibly scheduled with some, or all of the VLA antennas while they are in the **A**-configuration. To demonstrate the differences in imaging performance, we simulated two situations which should be representative of the range of possibilities – correlation of all New Mexico Array antennas with all 27 VLA antennas, and with the four VLA antennas located at the center of the array and end of each arm.

3 Calculations of the Imaging Characteristics

Justification of any proposed array design must be based on its ability to reconstruct a complicated image under a wide range of possible observing parameters, including declination and observing duration. We chose to use as the trial model a λ20-cm image of the galactic SNR Cassiopeia A, made with all four configurations of the VLA. This is a large and complex image, comprising over 10^6 independent pixels, with a dynamic range exceeding 4000:1, and a range of spatial scales of about 300. We believe it is important to judge imaging performance on the basis of such a complex image, as it is imaging fidelity over a very large angular range, as well as sensitivity, which the EVLA promises to provide.

In order to impart some realism to the simulations, the trial image was 'moved' to the distance of the Andromeda galaxy by reducing its angular scale by a factor of 250. At this distance, Cassiopeia A would have an angular diameter of 1.6 arcseconds and a spectral flux density of 35 mJy. Imaging of a 35 mJy extended object by the EVLA would be noise-limited, so we multiplied the 'true' flux density by a factor of 100 to ensure adequate SNR for these imaging trials. The trial image is shown in Figure 3, at its native resolution of 5.6 mas. The total spectral flux density is 3.5 Jy at 20cm.

The trials we performed were made at a frequency of 8.4 GHz, where the EVLA will provide a resolution of about 20 mas. This provides about 6400 independent resolution elements across the model, sufficient to determine the imaging characteristics of the proposed configurations. A full resolution trial for the model image would require 'observing' at a frequency of about 30 GHz. Simulations at this frequency and resolution combination will be attempted later.

The trial databases were made using the `AIPS` program `UVCON`, written by L. Kogan. This program produces an `AIPS` UV database containing the calculated visibilities for an array with specified geometry and sensitivity, using an input trial image. The program permits inclusion

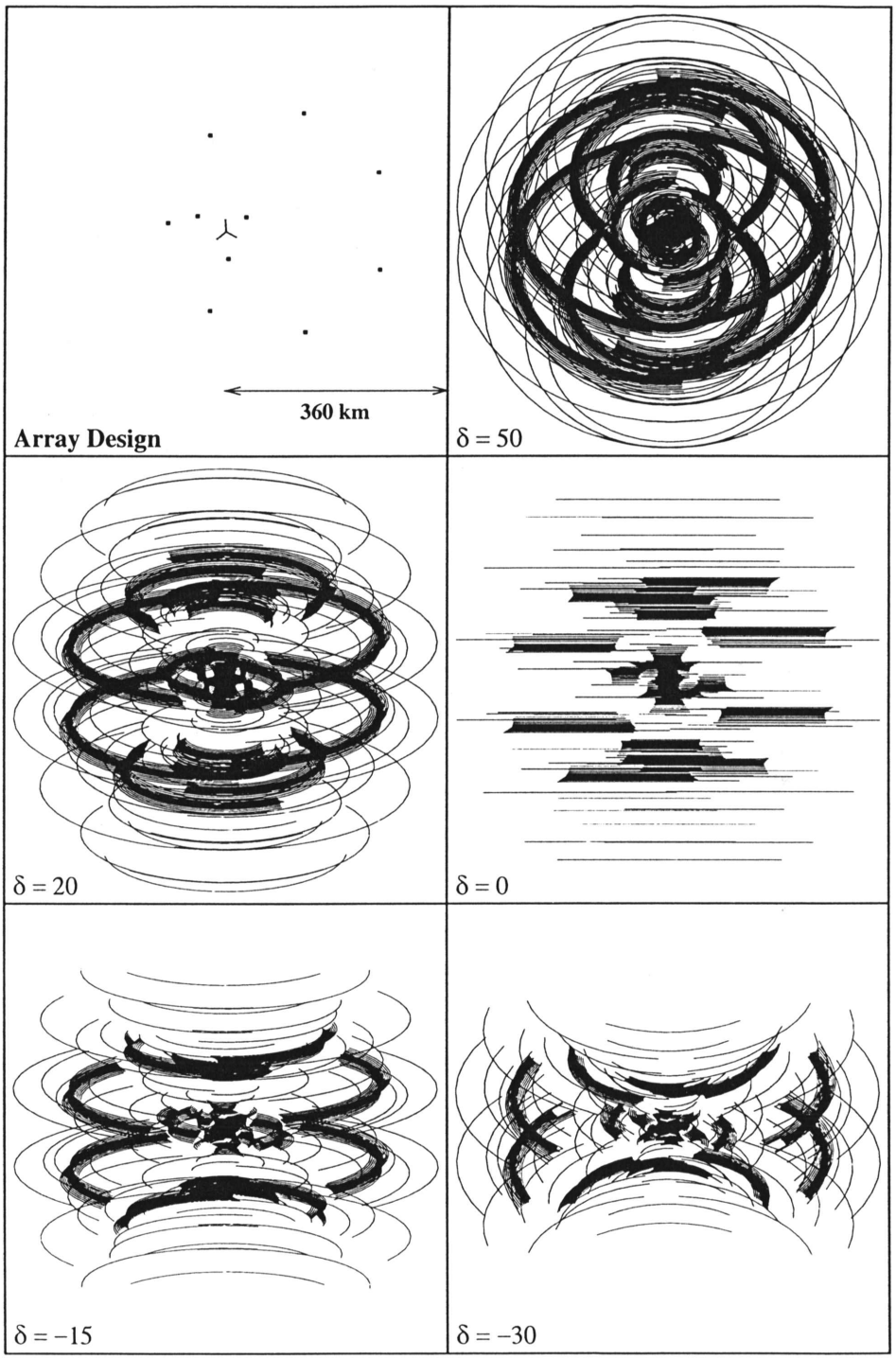

Figure 1: The EVLA geometry with $N = 8$ used for these simulations, and the uv-coverag
a full synthesis at various declinations. The scale in the upper left panel applies to all pa
All 27 VLA antennas, plus the VLBA antennas at Pietown and Los Alamos, are included.

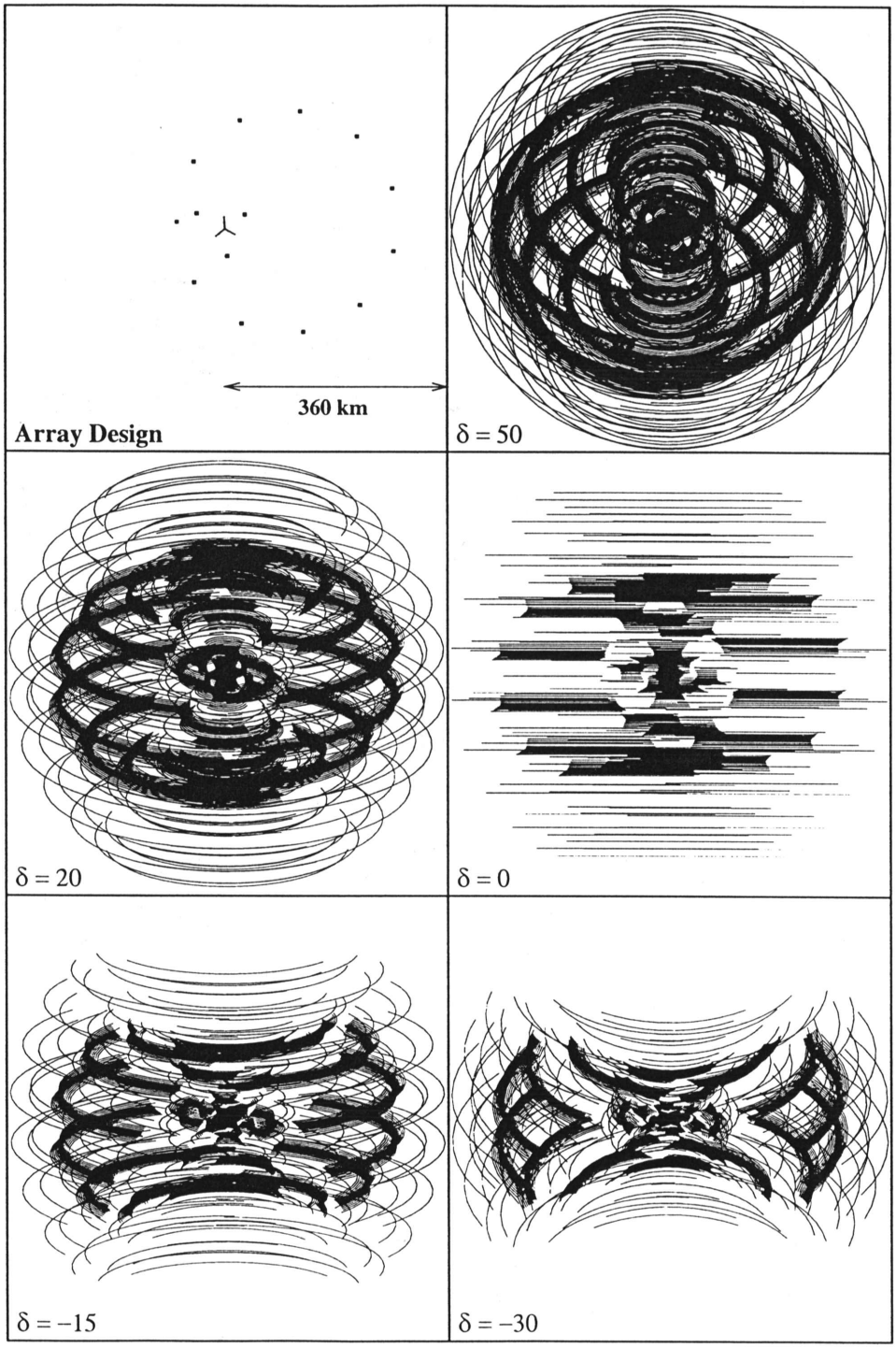

Figure 2: The EVLA geometry with $N = 12$ used for these simulations, and the *uv*-coverage of a 12-hour synthesis at various declinations. The scale shown in the upper left panel applies to all panels. All 27 VLA antennas, plus the VLBA antennas at Pietown and Los Alamos, are included.

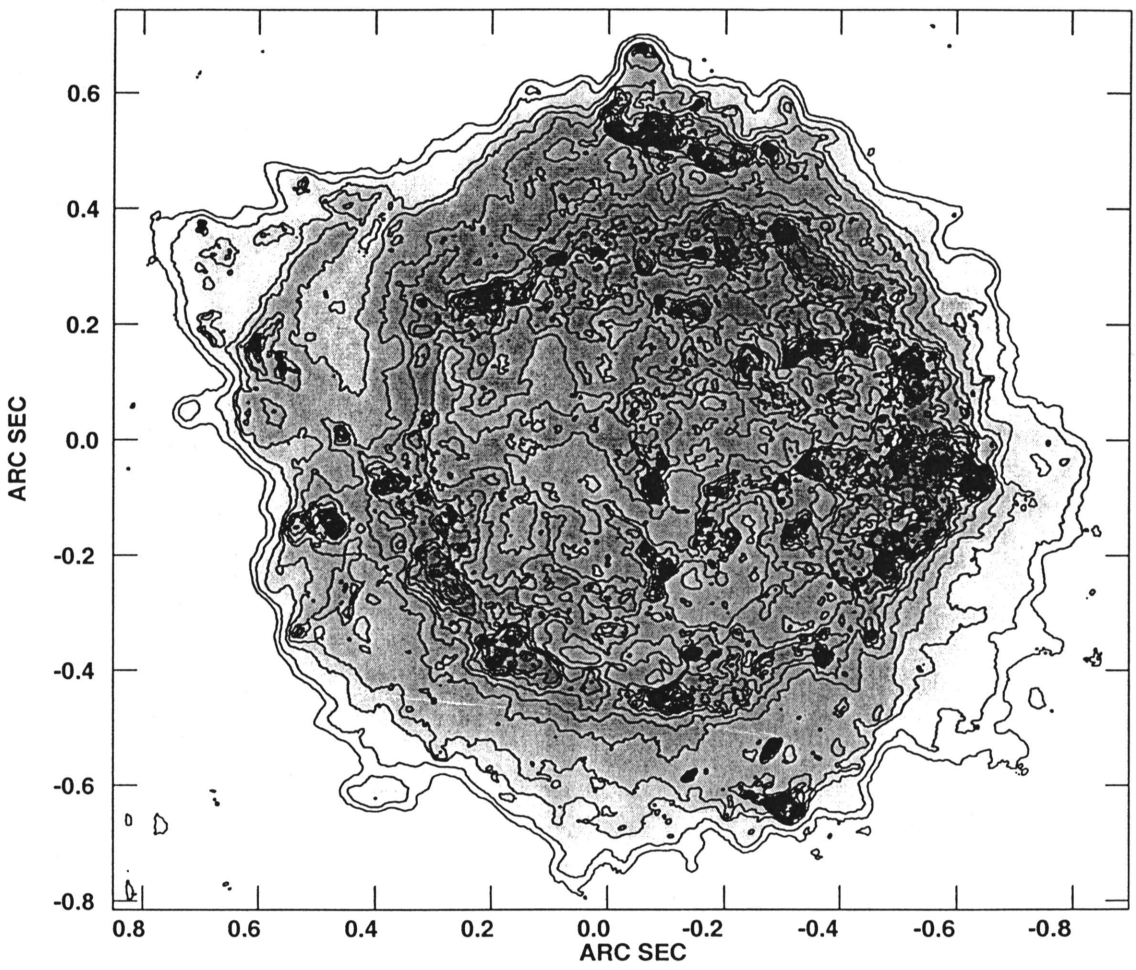

Figure 3: The model used in the simulations. This is a 20cm image of Cassiopeia A, made using data from all four VLA configurations, and smoothed to a resolution of 1.45 arcseconds. The scale was then reduced by a factor of 250 to simulate the appearance of a similar SNR at the distance of the Andromeda galaxy. The effective resolution of this image is then 5.8 milliarcseconds. The brightness has been adjusted to a level 100 times that of Cas A, in order to ensure the simulations are not noise-limited. The contours shown are at -0.1, 0.1, 0.5, 2.5, 5, 10 ... 95% of the peak brightness of 0.63 mJy/beam.

of various errors, including thermal noise, random and global pointing errors. We have included thermal noise, with parameters appropriate for the sensitivity of the EVLA, but have not attempted to estimate the effects of pointing errors as these will not be important for the angular size and frequency of these simulations. The program also permits simulation in a 'multi-frequency' mode, but without inclusion of spectral index gradients.

Simulated databases were made for nine standard declinations (δ = 80, 50, 30, 15, 5, 0, -5, -15 and -30) for each of 12 different array geometries. As described above, the array geometries differed by the number of new antennas – from 4 to 15. In all cases, two of these new antennas were fixed on the inner ring, with the rest uniformly distributed around the outer ring. The observing duration was set by an imposed elevation limit of ten degrees or, for nothern declinations, was limited to 12 hours centered at meridian transit.

The 108 simulation trials (9×12) were performed twice – once using the full complement of 27 VLA antennas, and once for a 4-antenna subset, comprising one antenna at the end of each A-configuration arm, and one antenna at the array center. In hindsight, it is clear that this last combination was poorly chosen – the minimum spacing available is about $0.5\mathrm{M}\lambda$ – with a fringe spacing of 0.25 arcseconds – far too large to recover the large-scale structure of the model. Hence, these simulated images were very poor, and we will not report on the quantifiable results, as they are dominated by the missing large-scale structures.

The AIPS program IMAGR was used to generate the images for each trial array and declination. Because of the heavy concentration of short spacings from the intra-VLA antennas, the robust weighting parameter was set to -2. The AIPS program VTESS was employed to deconvolve the image.

As will be shown below, imaging performance for objects near the equator is considerably degraded compared to the performance for northern objects. The cause of this phenomenon is very clear – the spatial frequency sampling tracks are very nearly horizontal, so that earth rotation is only effective in extending the (u,v) coverage in one dimension, rather than two at higher (and lower) declinations. The only effective means of improving imaging performance is to employ a bandwidth synthesis mode, whereby data are taken over a wide range in frequency. It is expected that this mode of observing (for continuum objects) will be very commonly employed. Testing this mode is quite expensive in computer time, and we have performed only two trials, whose results are given at the end of this report.

From each simulation we calculated the rms thermal noise, the effective solid angle of the synthesized beam, the peak difference between the original model (convolved to the same resolution as the reconstruction) and the reconstructed image, the on-source rms difference between the (convolved) original and reconstructed images, and a fidelity index generated by dividing the peak brightness of the (convolved) model image by the on-source rms difference between the model and image. These latter two quantities are particular useful measures of the imaging fidelity. Figure 4 shows a montage image illustrating these key quantities: The upper left shows the model image convolved to the 20 mas resolution of the trials, the upper right shows the reconstructed model for a declination of 50 degrees, with $N = 8$, the bottom left shows the difference between the simulation image and the model, and the bottom right the ratio between the difference and the model. This last panel thus shows the actual *fractional error* in the reconstruction.

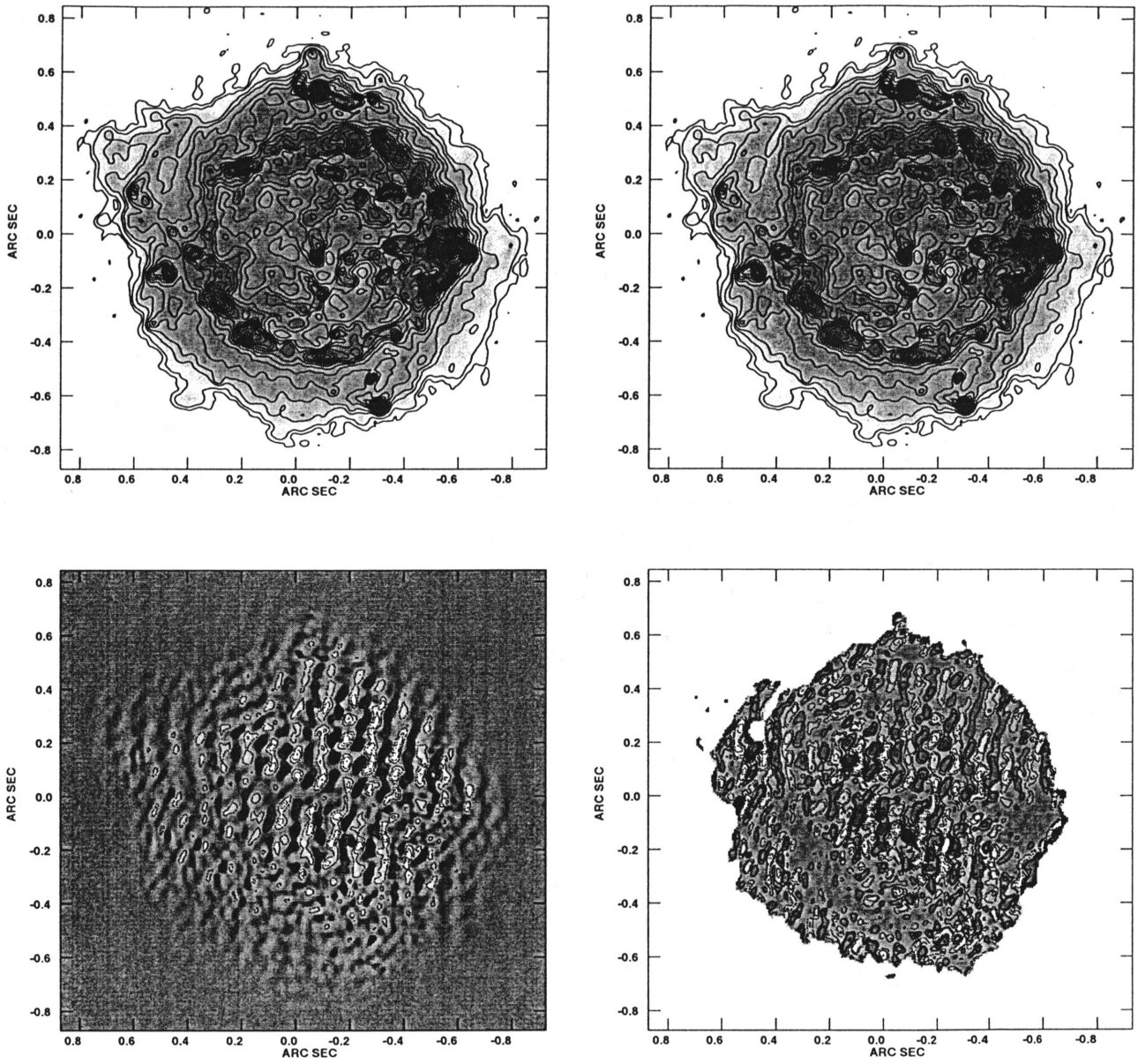

Figure 4: A sequence of images showing the model, the synthesized test, and two views of the errors. The upper left shows the 'truth' image – the model image convolved to the 20 mas resolution of the simulation. The upper right shows the result of the simulation for $\delta = 50$, using one frequency channel at 8.4 GHz. The brightness has been reduced by 50% from the 20cm value to account for the spectral index. For both panels, the greyscale wedge runs from -3 μJy/beam to 2.5 mJy/beam, and the contour levels are at -0.1, 0.1, 0.5, 2.5, 5, 10, ..., 95% of the peak of 2.8 mJy/beam. The bottom left panel shows the error image – the difference between the model and the trial. The linear greyscale wedge runs from -75 to $+75$ μJy/beam, and the contours are at ± 75, ± 37, ± 25 μJy/beam. The lower right panel shows the ratio between the error image and the model – this is the fractional error in the simulation image. For this panel, the linear greyscale wedge runs from -25 to $+25$%, with contour levels at ± 20, ± 15, ± 10, ± 5, and ± 2.5%. The mean fractional error in this simulation is 5.5%.

4 Simulation Results and Discussion

The key results of the study are shown in Figures 5 through 8. These show the resolution, point-source sensitivity, rms error in the simulated image, and the fidelity index. For the first two, we have also displayed the results from the set of 4-VLA antenna trials, as these do not reflect the poor imaging characteristics caused by severe over-resolution of the model.

We comment on these results in the following tabulation.

- **Effective Beam Area**

  Figure 5 shows the effective solid angle of the synthesized beam, in milliarcs^2. The 27-VLA antenna trials are shown with black dots, the 4-VLA antenna trials with open squares. The former set has lower resolution because of the effect of the large number of short, intra-VLA spacings. Weighting schemes can largely offset this effect of these short spacings, but only at a severe cost in sensitivity. We have chosen a single robustness of -2, which leads to the relations shown in the figure. The resolution improves with increasing number of new (outer) antennas, as their long spacings increasingly dominate the effective resolution.

- **Point-Source Sensitivity**

  Figure 6 shows the variation in sensitivity for the simulations. The curves reflect only the expected effects of the number of antennas and integration time involved in each simulation. Sensitivity improves with increasing numbers of antennas, and with increasing declination.

- **RMS Image – Model Difference**

  Figure 7 shows the on-source r.m.s. differences between the model and output image. For all, the improvement with number of outer antennas is clear. Only the results from the 27-VLA antenna trials is shown, as the 4-VLA antenna trials greatly over-resolved the model image.

- **Fidelity Index**

  Figure 8 shows a measure of the fidelity – the ratio of the peak model image brightness to the rms errors in the reconstruction. The poor imaging performance near $\delta = 0$ is due to the baseline loci travelling horizontally in the $u - v$ plane, thus reducing the number of unique sample points available to the array. The relatively poorer performance at far southern declinations merely reflects the obvious fact that the sources are not above the horizon long enough to permit the dense sampling required for very high-fidelity imaging.

5 Imaging Improvements from Bandwidth Synthesis

The rather poor imaging performance near the equator is an expected result, as the u-v sampling due to earth-rotation is only effective in one dimension. Other than packing more antennas into the outer ring, there is no way obtain the type of performance we find at higher declinations.

But a considerable improvement can be obtained through use of 'bandwidth synthesis' – observing a (continuum) source over a wide range of frequencies, and performing a joint deconvolution to produce both the image, and the spectral index across the bandwidth utilized. This method will, of course, improve the high-declination imaging performance as well. It is most critically needed at these low declinations.

The AIPS program UVCON has a rudimentary means of producing a 'bandwidth-synthesis' mode of observing – it will calculate the visibilities at equally spaced frequencies over some defined range. No spectral variations can be input, so the trials are necessarily confined to objects with a uniform spectrum. On the other hand, the technique for fully deconvolving the structure and spectrum has been only rudimentally developed – this is an important area needing further imaging research.

In view of these limitations, the results shown below must be regarded as optimistic. Nevertheless, they are very encouraging.

To obtain an impression of the degree of improvement we can expect, we synthesized four cases for two declinations, using the $N = 8$ configuration only. The four cases are a single frequency, two frequencies separated by 20% of the center frequency, four frequencies each separated by 10% of the center frequency (thus a total span of 30%), and 8 frequencies, each separated by 5% of the center (thus spanning 35%). All trials used the same center frequency, and the same total bandwidth. The results are shown in Figures 9 and 10.

Figure 9 shows the results for $\delta = 0$. The four panels show the fractional errors in the simulations for the four trials. The improvement between the single-frequency trial and the others is dramatic. The mean fractional error in the four trials are 14, 8.9, 2.5, and 2.1%. The reduced rate of improvement between the four-frequency and eight-frequency siulations indicates that it is fractional bandwidth coverage which is important – as expected.

Figure 10 shows the same results for $\delta = 50$. The imaging at this declination is much more precise than at $\delta = 0$ – the greyscales are set four times lower. The mean fractional errors are 5.5, 1.3, 0.6, and 0.5%. Again, there is little improvement between the 4-frequency and 8-frequency case – as might be expected since the fractional frequency span increases only slight – from 30% to 35%.

6 Summary

There are no surprising results reported in this study. We find that more antennas, and more frequencies, lead to better imaging. There is no indication of a roll-off in the improvement in the fidelity index with increasing numbers of antennas for imaging a highly complex structure. Preliminary indications are that the fractional bandwidth used is the key parameter for bandwidth synthesis. None of the above conclusions are surprising. Our major goal has been to establish a methodology for quantifying imaging capabilities for the EVLA, and to give some quantitative basis for discussing the relative value of various numbers of new antennas in any extended array.

This work is only the beginning of a proper study. We have made no attempt to optimize antenna locations, nor were we constrained by any practicalities in locating antennas. These results must be extended by comparing these results to other suggested array geometries. We must also better explore the improvements offered by bandwidth synthesis techniques – but

keeping in mind that spectral line observing cannot benefit from this technique. And, as snapshot modes of observing will certainly be used by the EVLA, studies of this imaging methodology must also be undertaken.

The authors wish to thank Leonia Kogan for his invaluable assistance, both for suggesting the configuration, and for writing the simulation program `UVCON`. We also are grateful to Larry Rudnick for providing the spectacular image of Cassiopeia A.

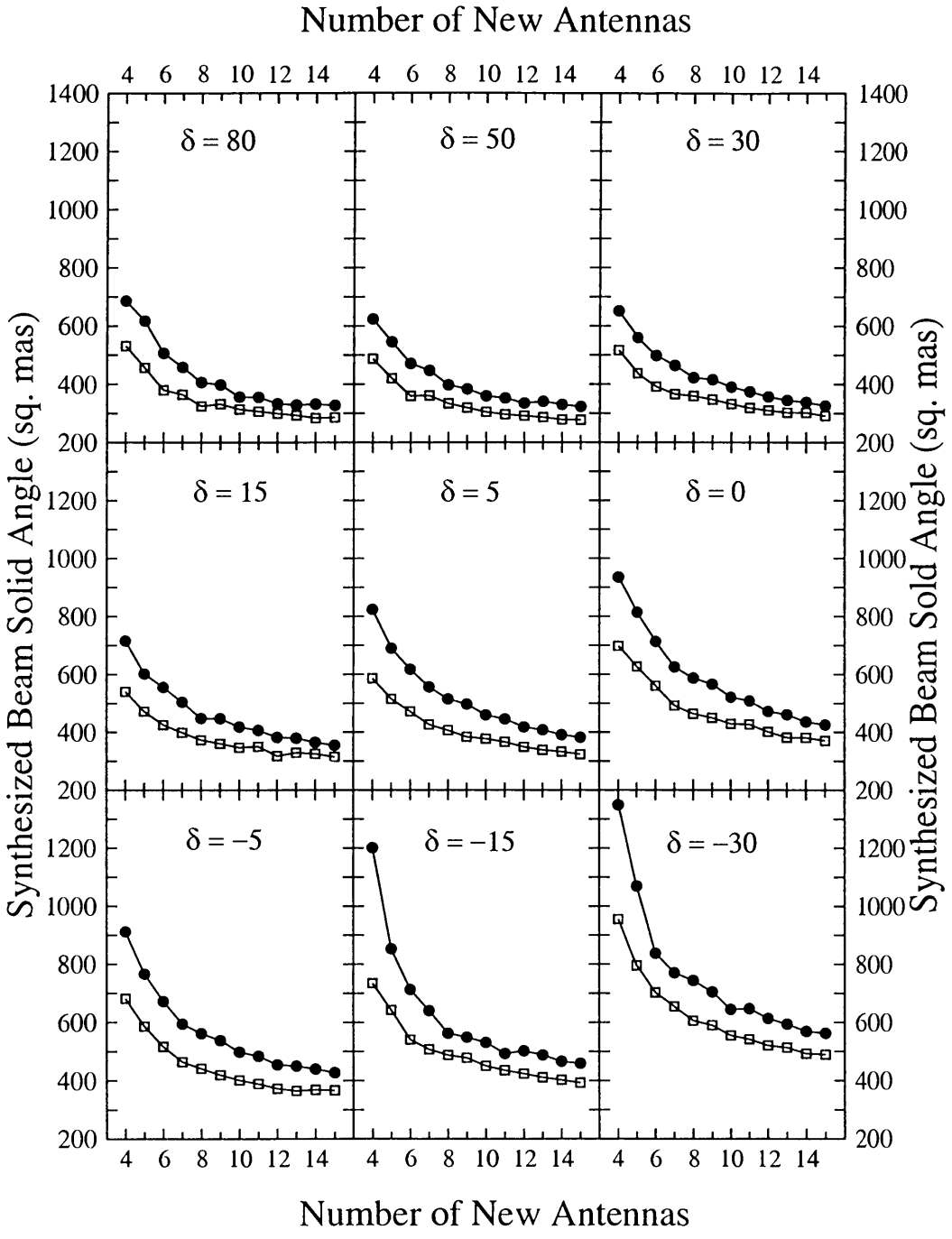

Figure 5: The effective resolution of the synthesized beam at 8.4 GHz as a function of the number of new antennas. Each chart is for a different source declination. The 27-VLA antenna simulations are shown with black dots, the 4-VLA antenna simulations are shown with open squares. Both sets of simulations include the Pietown and Los Alamos antennas.

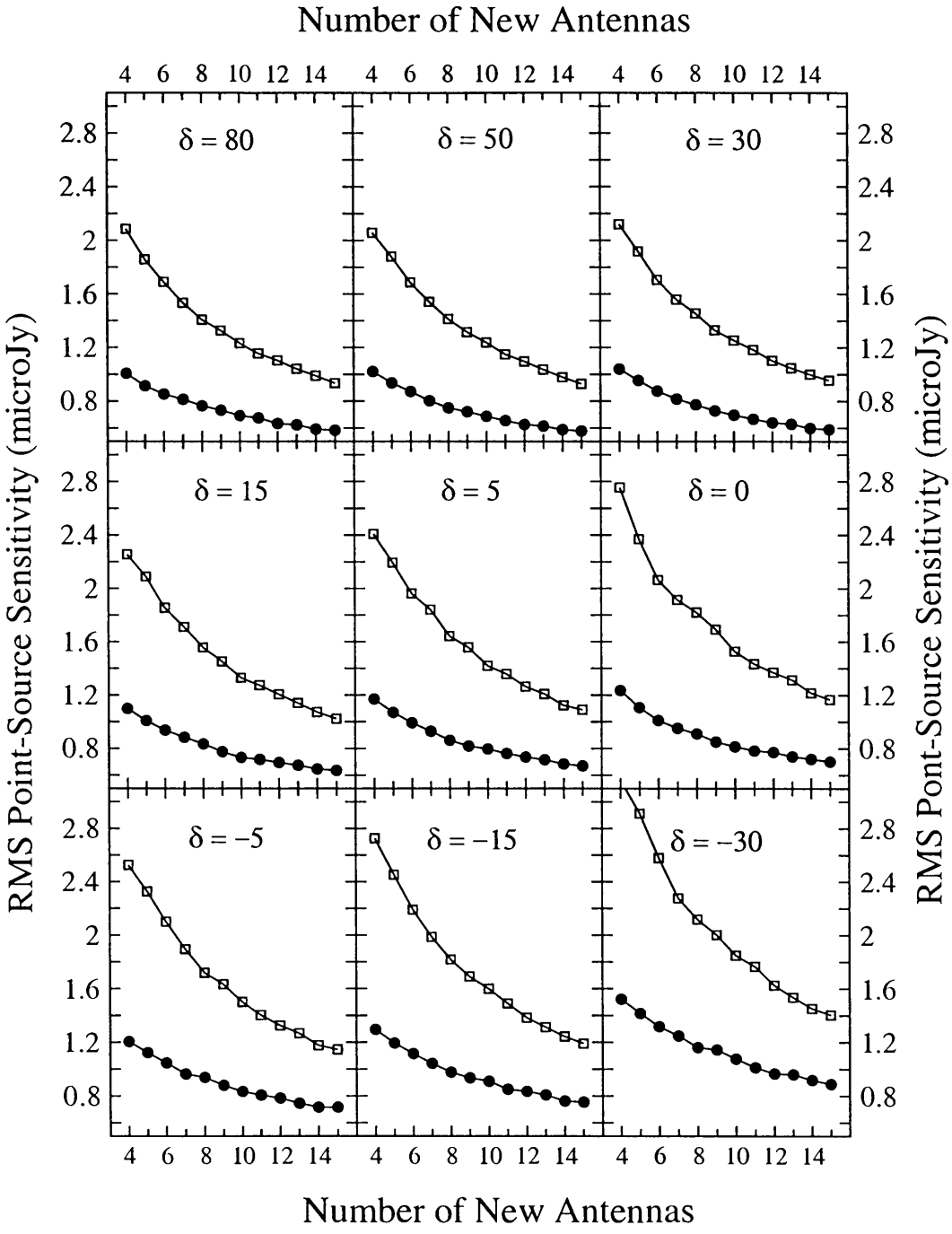

Figure 6: The RMS noise in the simulations, assuming a total bandwidth of 4 GI receiver and correlator parameters expected for the EVLA at 8.4 GHz frequency The VLA is shown with black dots, the 4-antenna VLA in open squares.

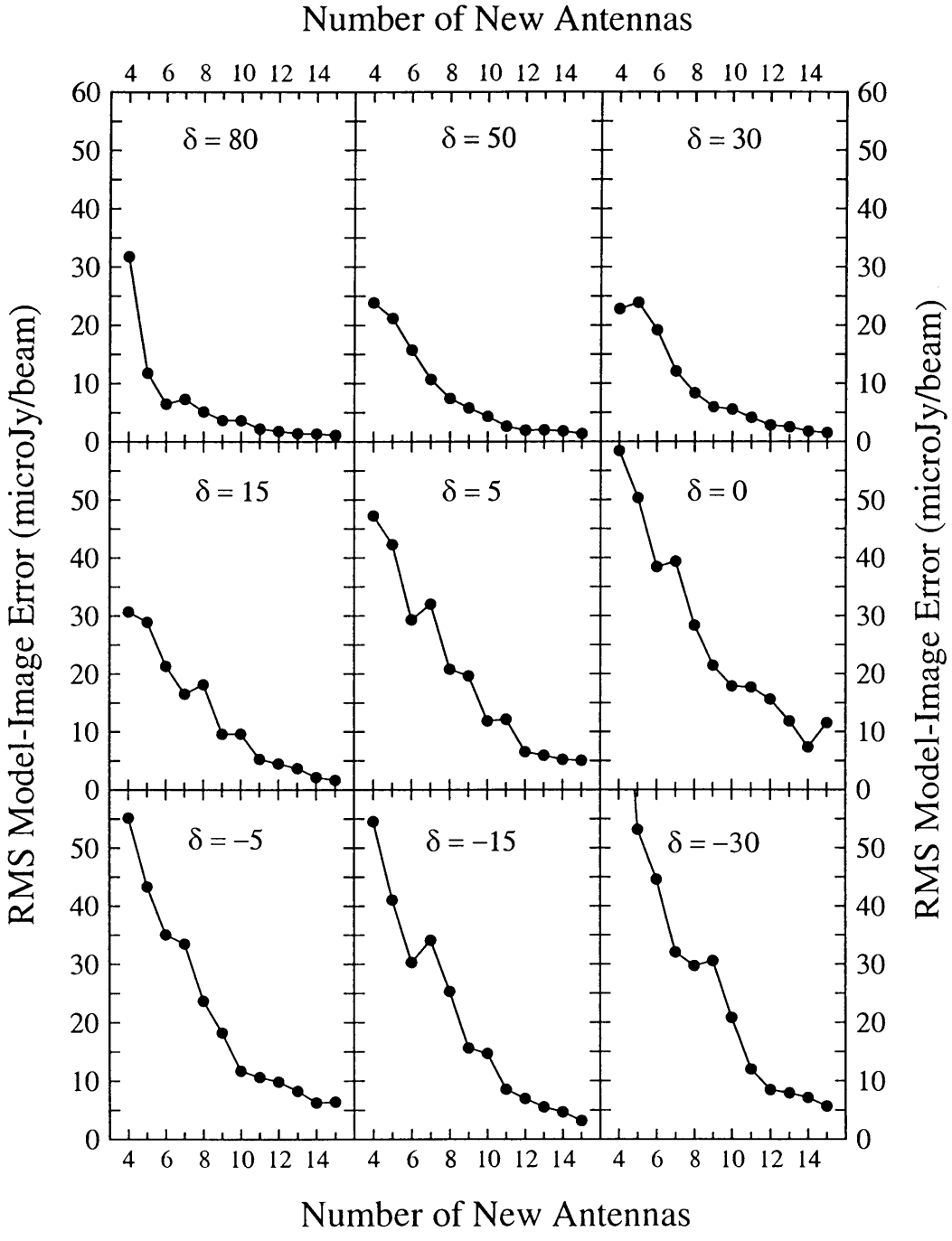

Figure 7: The on-source RMS difference between the model and the simulated resp function of the number of new antennas. The full VLA, PieTown, and Los Alamos ar

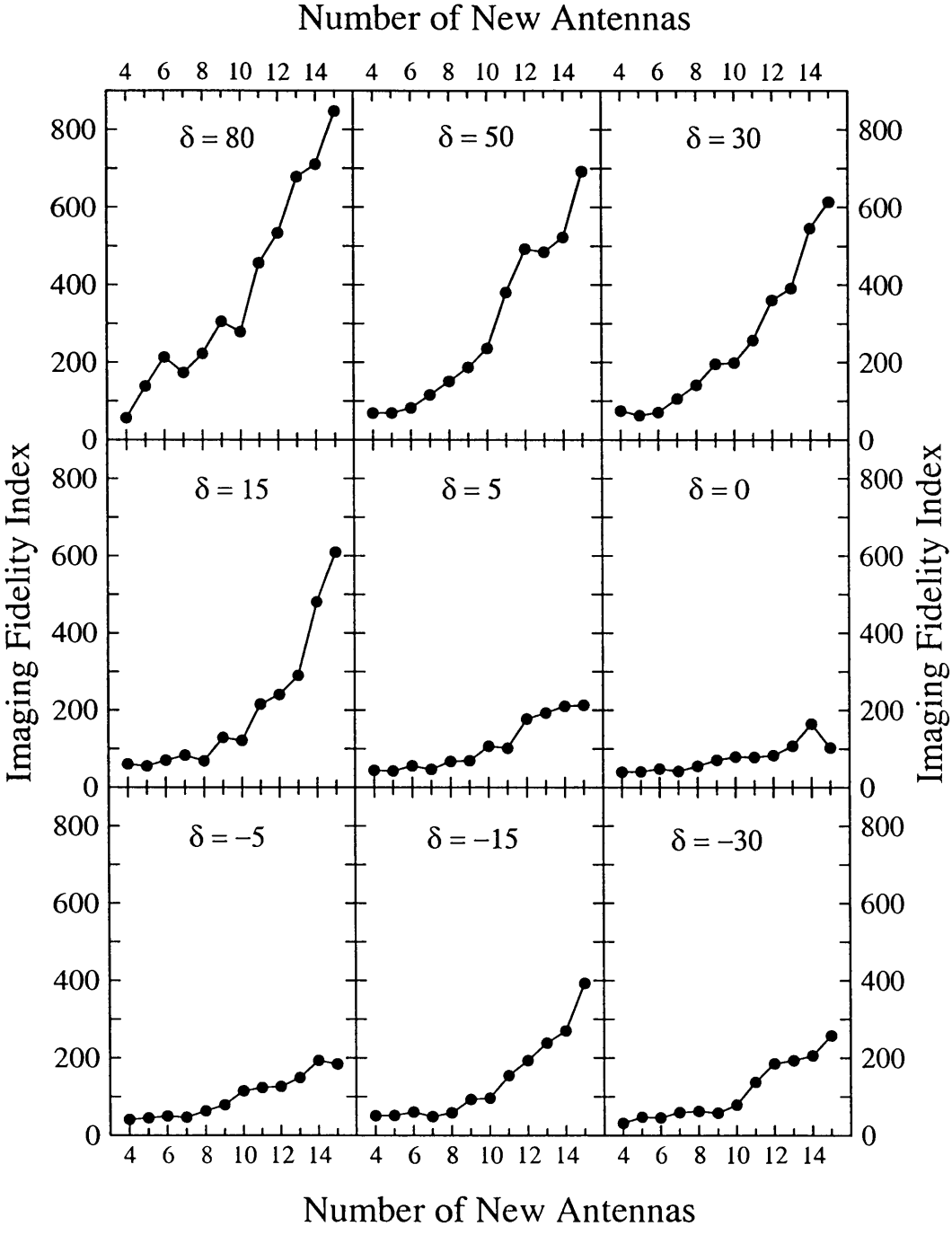

Figure 8: The fidelity of the simulation, with 27 VLA antennas, for the nine declinations. The fidelity is defined as the peak in the model divided by the rms error of the difference between model and simulation.

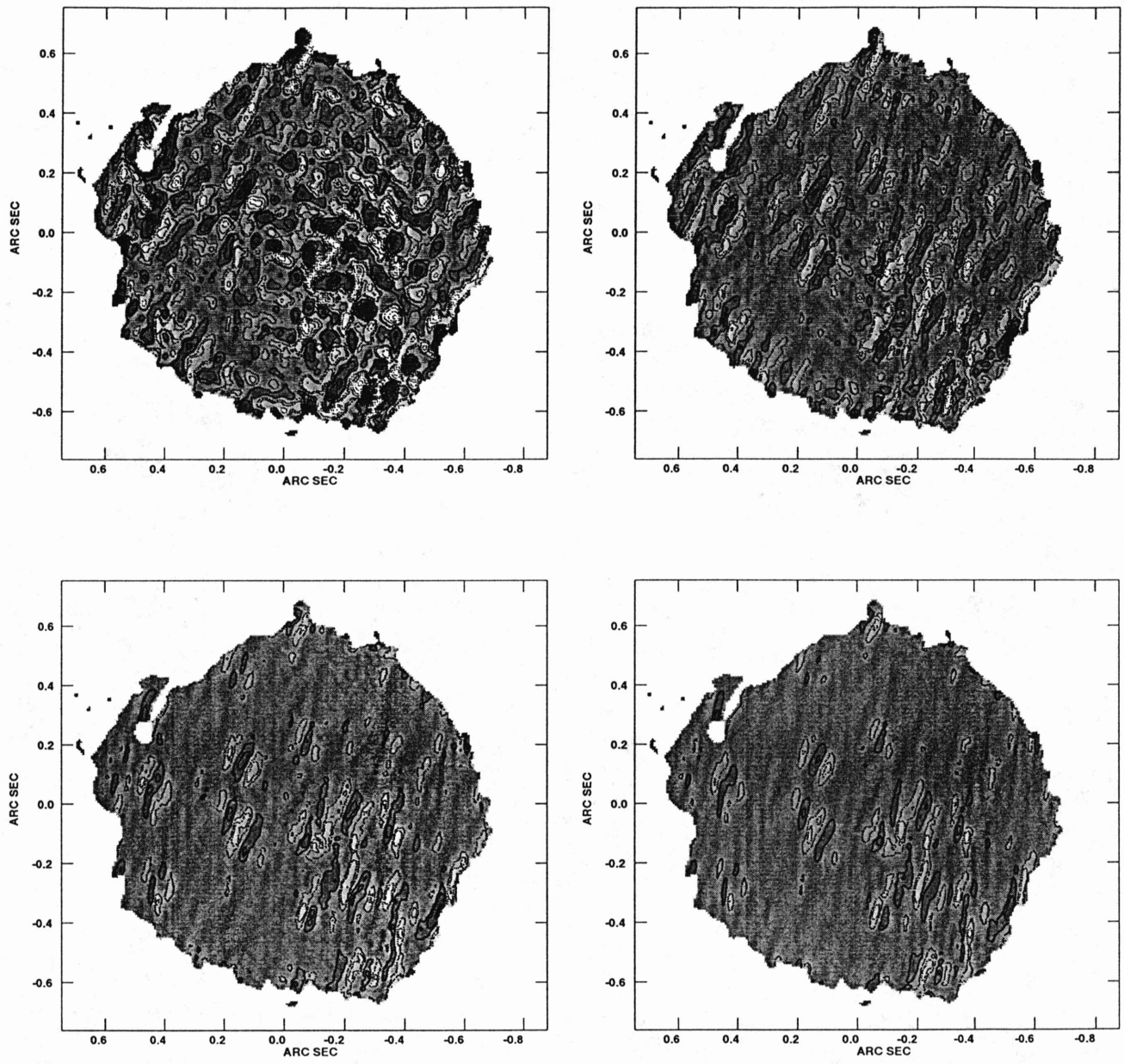

Figure 9: The fractional error in the simulation for $\delta = 0$, with the eight-antenna configuration and a single frequency (upper left), two frequencies spread over 20% (upper right), four frequencies spread over 30% (lower left), and four frequencies spread over 35% (lower right). The linear greyscale runs between -40 and $+40$ %. The contour levels are at ± 60, ± 50, ± 40, ± 30, ± 20, ± 10, and ± 5%. The mean errors are 14, 8.9, 2.5, and 2.1% for the four trials.

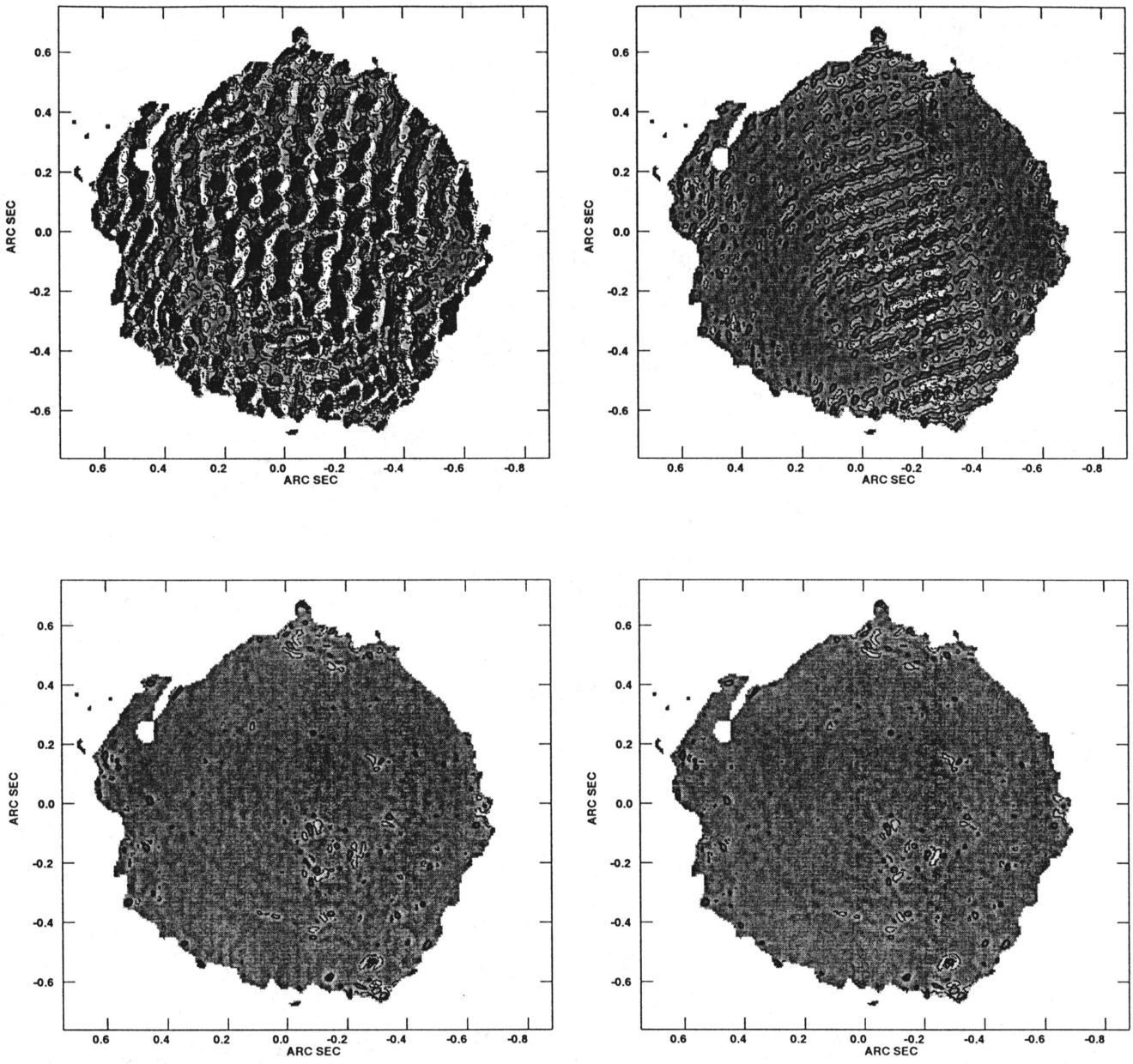

Figure 10: The fractional error in the simulation for $\delta = 50$, with the eight-antenna configuration and a single frequency (upper left), two frequencies spread over 20% (upper right), four frequencies spread over 30% (lower left), and four frequencies spread over 35% (lower right). The linear greyscale runs between -10 and $+10$ %. The contour levels are at ± 40, ± 30, ± 20, ± 10, ± 5, ± 2.5 and ± 1%. The mean errors are 5.5, 1.3, 0.58, and 0.56% for the four trials.